R. & M. No. 3630

R. & M. No. 3630

MINISTRY OF TECHNOLOGY

AERONAUTICAL RESEARCH COUNCIL
REPORTS AND MEMORANDA

The Linearised Subsonic Flow over the Centre-Section of a Lifting Swept Wing

By PATRICIA J. ROSSITER
Aerodynamics Dept., R.A.E., Farnborough

LIBRARY
ROYAL AIRCRAFT ESTABLISHMENT
BEDFORD

LONDON: HER MAJESTY'S STATIONERY OFFICE
1970
PRICE 18*s* 0*d* [90*p*] NET

The Linearised Subsonic Flow over the Centre-Section of a Lifting Swept Wing

By PATRICIA J. ROSSITER

MINISTRY OF TECHNOLOGY

Reports and Memoranda No. 3630*
April, 1969

Summary.

The linearised equation for the velocity potential of subsonic flow past a semi-infinite plane sector has eigensolutions. These determine the singular behaviour of the loading, according to the linearised theory of subsonic flow, at the leading and trailing edges of the centre-section of a swept wing. The eigensolutions are proportional to a positive power of the distance from the apex of the sector. Values of the exponents of this factor for the first two eigensolutions are calculated as functions of the apex angle, using a finite-difference approximation to the partial differential equation. The first of these corresponds to the strength of the singularity in the loading at the apex of a swept wing and the second, which is compatible with the Kutta-Joukowski condition, describes the rate at which the loading tends to zero as the trailing-edge root is approached.

LIST OF CONTENTS

*Replaces R.A.E. Technical Report 69 072—A.R.C. 31 369.

---

1. *Introduction.*

According to the linearised theory of subsonic flow, the loading on a lifting swept wing is singular along the leading edges, including the apex, and zero at the trailing edges. It is well known that the loading tends to infinity like the reciprocal of the square root of the distance from the leading edge, and to zero like the square root of the distance from the trailing edge, except at points where the edge has discontinuous slope. This Report examines the behaviour of the linearised solution for the subsonic flow over a lifting swept wing in the regions near the landing and trailing edges of the centre-section, where the edges have discontinuous slope.

By considering the problem in a stretched co-ordinate system, it can be shown that in both regions the velocity potential for this problem is dominated by a term which is an eigensolution of the equation and the boundary conditions which govern the velocity potential of subsonic flow past an infinite plane sector.

Germain[1] has shown that the equation for the latter velocity potential has an infinity of eigensolutions of the form

$$\phi_m = r^{\nu_m} f_m(\vartheta, \omega)$$

with $\nu_m \geqslant 0$, where r is the distance from the apex of the sector, f_m a function of the polar angles ϑ and ω, and ν_m depends only on the apex angle of the sector.

The strength of the singularity in the loading at the apex of the wing corresponds to the eigensolutions with

$$0 < \nu_m < 1,$$

and Germain[1] has shown that there is just one eigenvalue in this interval for all values of the semi-apex angle of the wing, γ. This eigenvalue ν_0 is a continuous function of γ and decreases monotonically with γ, being one when $\gamma = 0$, 0·5 when $\gamma = \pi/2$, i.e. when the wing is unswept, and zero when $\gamma = \pi$.

The first attempt to find ν_0 for a general value of γ was made by Legendre[2], who expanded ν_0 for γ near $\pi/2$ as a power series in $\cos\gamma$ and calculated the first three terms. Guiraud[3] obtained two terms of a

power series expansion in $(1-\cos\gamma)$ for γ near zero. Brown and Stewartson[4] have also calculated power series expansions for γ near $\pi/2$ and for γ near zero, by a systematic technique, and in each case have obtained a further term. The expansions are, for γ near $\pi/2$,

$$\nu_0 = \tfrac{1}{2}+\frac{1}{\pi}\cos\gamma+\frac{1}{\pi^2}\cos^2\gamma+\left(\frac{1}{\pi^3}+\frac{1}{6\pi}\right)\cos^3\gamma+0\,(\cos^4\gamma)$$

and for γ near 0,

$$\nu_0 = 1-\tfrac{1}{2}(\sec\gamma-1)+\{\tfrac{1}{4}(\sec\gamma-1)^2\log(\sec\gamma-1)+\tfrac{3}{4}(1-\log_e 2)(\sec\gamma-1)^2\}$$
$$+0\,[(\sec\gamma-1)^3\log^2(\sec\gamma-1)]\,.$$

Values obtained from these series are tabulated in Table 1 and shown graphically in Fig. 12.

A numerical method for calculating values of ν_m for any angle γ is given in this Report. In Section 2, it is shown that ν_m is an eigenvalue of a two-dimensional partial differential equation with homogeneous boundary conditions in a semi-infinite domain. The method of solution for ν_m is given in Section 3, and entails using a transformation of variables to make the domain of the problem a rectangular region. By approximating the partial differential equation by a finite difference equation at each point of a rectangular mesh, λ_m, where

$$\lambda_m = \nu_m(1+\nu_m)$$

is shown to be an eigenvalue of a known matrix, and the required eigenvalue can be found from an initial approximation. This eigenvalue depends, of course, on the order of the matrix, which is related to the size of the finite difference mesh. By calculating eigenvalues for smaller and smaller meshes, it is possible to estimate the eigenvalues of the differential equation by extrapolation. Accurate values are obtained using coarse meshes for γ near $\pi/2$, but for γ very near 0 or π the extrapolation cannot be relied on.

Results for ν_0 are given in Tables 1 and 2, and Figs. 10, 11 and 12, and are discussed in Section 4. They agree closely with results obtained by Brown and Stewartson[4], who use a different numerical method based on the eigenvalues of a pair of ordinary differential equations obtained by separation of the variables. In the R.A.E. standard method, the load on the centre-section has a similar singularity at the apex, but the exponent varies linearly with γ between the same limits, as shown in Fig. 12.

The flow at the apex of the wing is dominated by the eigensolution with the smallest exponent ν_0, and the other eigensolutions of the infinite sector problem are therefore of less interest. However, the method has been used to find the next eigenvalue ν_1 for two values of γ less than $\pi/2$, and these results are given in Section 4.

In the case of the trailing edge, the dominant term in the velocity potential is the eigensolution with smallest exponent which is compatible with the Kutta-Joukowski condition. This states that the streamwise derivative of the velocity potential must be finite at the trailing edge, and means we must have

$$\nu_m \geqslant 1\,.$$

The smallest such ν_m, denoted by ν_1, represents the rate at which the loading tends to zero at the centre-section of the trailing edge, and has been found for a large range of angles of sweepback of the trailing edge. The results are given in Section 4, Table 3 and Figs. 13 and 14. Included in the former figure are the analytical values $\nu_1 = 1{\cdot}5$ for an unswept trailing edge, and the limiting value $\nu_1 = 1$ for a trailing edge with angle of sweepback $\pi/2$.

2. *Formulation of the Problem.*

2.1. *Basic Equations of the Flow.*

We consider the linearised approximation to the inviscid subsonic flow past a lifting swept wing. By a Prandtl-Glauert transformation this may be reduced to a consideration of the inviscid, incompressible flow past a related swept wing and, by virtue of the linearity, the lifting problem may be separated from the thickness problem.

We introduce the right-handed rectangular Cartesian co-ordinates $0x_1x_2x_3$ with $x_3 = 0$ as the plane of the wing and $x_2 = 0$ as the plane of symmetry of the flow, and seek a disturbance velocity potential $\Phi(x_1, x_2, x_3)$. This is a harmonic function which satisfies the following boundary conditions:

(a) Since on the wing the overall normal component of velocity is zero, $\partial\Phi/\partial x_3 = -U\alpha(x_1, x_2) = \omega(x_1, x_2)$, say, on the planform in the plane $x_3 = 0$, where $\alpha(x_1, x_2)$ is the slope of the camber surface of the wing and U is the undisturbed speed.

(b) By symmetry, Φ is an even function of x_2.

(c) Since Φ and $\partial\Phi/\partial x_1$ are odd functions of x_3 and $\partial\Phi/\partial x_1$, which is proportional to the pressure in the linear approximation, is continuous at points off the wing planform, $\partial\Phi/\partial x_1 = 0$ off the planform in the plane $x_3 = 0$.

So, in the plane $x_3 = 0$, except on the wing and wake, $\Phi = 0$, by integration from infinity upstream.

(d) Similarly, in the plane $x_3 = 0$, on the wake, Φ is a function of x_2 only, i.e. $\Phi = f(x_2)$.

(e) By the Kutta-Joukowski condition, $\partial\Phi/\partial x_1$ is continuous at the trailing edge.

(*f*) $\nabla\Phi$ tends to zero at infinity, except in the wake of the wing.

We wish to examine the behaviour of Φ near the landing and trailing edges of the centre-section of the wing. At these two points, the planform has a corner, which can be regarded as the apex of either the wing or the wake. In each case, we take the apex as the origin 0 and direct the axis $0x_1$ from the apex on to the planform, *see* Fig. 1. We denote by γ the angle between the direction $0x_1$ and the tangent at 0 to the edge we are interested in.

We now introduce stretched co-ordinates

$$(y_1, y_2, y_3) = (x_1/\varepsilon, x_2/\varepsilon, x_3/\varepsilon), \tag{2.1}$$

put

$$\Phi(x_1, x_2, x_3) = \phi_\varepsilon(y_1, y_2, y_3) \tag{2.2}$$

and look for a limit of ϕ_ε as ε tends to zero

$$\phi(y_1, y_2, y_3) = \lim_{\varepsilon \to 0} \phi_\varepsilon(y_1, y_2, y_3). \tag{2.3}$$

Then the behaviour of ϕ should reflect that of Φ near 0.

Since Laplace's equation is homogeneous in (x_1, x_2, x_3), ϕ is also a harmonic function. In each case, the planform becomes an infinite sector of angle 2γ, *see* Fig. 2. The following boundary conditions on ϕ are obtained by considering conditions (a) to (f) above as ε tends to zero:

(A) Since
$$\frac{\partial\phi_\varepsilon}{\partial y_3} = \frac{\partial\Phi}{\partial x_3}\frac{\partial x_3}{\partial y_3} = \varepsilon\frac{\partial\Phi}{\partial x_3} = \varepsilon\,\omega(x_1, x_2)$$

on the planform by condition (a), we have

$$\frac{\partial\phi}{\partial y_3} = 0 \text{ for } y_3 = 0 \text{ and } \frac{|y_2|}{\tan\gamma} < y_1. \tag{2.4}$$

(B) ϕ is symmetrical about $y_2 = 0$. (2.5)

Condition (c) will apply only to the wing apex case and becomes

(C) $$\phi = 0 \text{ for } y_3 = 0 \text{ and } \frac{|y_2|}{\tan\gamma} > y_1 . \tag{2.6}$$

Conditions (d) and (e) apply only to the case when 0 is the apex of the wake. In the limit $\varepsilon \to 0$, condition (d) implies

$$\phi = f(0) \text{ for } y_3 = 0 \text{ and } \frac{|y_2|}{\tan\gamma} > y_1 .$$

However, as the potential is unique only to an additive constant, we can take $f(0)$ as zero without loss of generality, and thus condition (C) also applies to the trailing-edge case.

(E) $\partial\phi/\partial y_1$ is continuous for $|y_2| = y_1 \tan\gamma$.

Condition (f) no longer applies, since, when ε tends to zero, points at infinity in the y-space arise from points at a finite distance in the x-space.

Germain[1] has shown that there exist eigensolutions of Laplace's equation satisfying the above conditions, in the form

$$\phi = r^{\nu} f\left(\frac{y_2}{y_1}, \frac{y_3}{y_1}\right) \tag{2.7}$$

where $r^2 = y_1^2 + y_2^2 + y_3^2$
and ν and f depend on γ. He expressed the problem in terms of integral equations and made use of a classical result (Chapter III 8.4 of Ref. 6) concerning the continuity properties of the eigenvalues and eigenfunctions of integral equations to show that the number of independent eigenfunctions associated with the eigenvalues ν in the interval $(p, p+1)$, where p is an integer, is independent of γ. By considering the problem for the case $\gamma = \pi/2$, Germain proves that there is just one eigenvalue ν_0 in the interval $(0, 1)$ for all γ. This takes the values $\nu_0 = 1$ for $\gamma = 0$, $\nu_0 = 0{\cdot}5$ for $\gamma = \pi/2$, and $\nu_0 = 0$ for $\gamma = \pi$.

Since any negative value of ν would correspond to a non-integrable singularity in the load on the wing, ν_0 is the smallest acceptable eigenvalue. On the other hand, eigensolutions corresponding to larger eigenvalues ν are dominated, for small r, by that corresponding to ν_0. Hence this eigenvalue $\nu_0(\gamma)$ describes the singular behaviour of the loading at the apex of a swept wing.

The eigensolutions relevant to the trailing edge case must satisfy the additional condition (E). This imposes the condition

$$\nu \geqslant 1 .$$

The eigensolution corresponding to the smallest such eigenvalue, ν_1, will be the dominant term in the velocity potential near the centre-section of the trailing edge, ν_1 determining the rate at which the loading tends to zero at that point.

2.2. *Derivation of Equation for* ν.

We introduce the system of orthogonal curvilinear co-ordinates (r, θ, τ) as defined by Legendre[2]

$$y_1 = \frac{r\cos\theta}{\cosh\tau} \qquad y_2 = \frac{r\sin\theta}{\cosh\tau} \qquad y_3 = r\tanh\tau \qquad r = (y_1^2 + y_2^2 + y_3^2)^{1/2} \tag{2.7}$$

and seek a solution of the form

$$\phi = r^{\nu} f(\tau, \theta) \tag{2.8}$$

of Laplace's equation

$$\frac{\partial^2 \phi}{\partial y_1^2} + \frac{\partial^2 \phi}{\partial y_2^2} + \frac{\partial^2 \phi}{\partial y_3^2} = 0. \tag{2.9}$$

We obtain a second order partial differential equation for f in the variables τ and θ in which ν appears as a parameter:

$$\frac{\partial^2 f}{\partial \tau^2} + \frac{\partial^2 f}{\partial \theta^2} + \frac{\nu(\nu+1)}{\cosh^2 \tau} f = 0. \tag{2.10}$$

The domain of the problem is the strip of the (τ, θ) plane where $|\theta| \leqslant \pi$ (*see* Fig. 3). The space $y_3 \geqslant 0$ corresponds to the area $\tau \geqslant 0, |\theta| \leqslant \pi$; the space $y_2 \geqslant 0$ to the area $0 \leqslant \theta \leqslant \pi$; and the wing to $\tau = 0$, $|\theta| \leqslant \gamma$. The boundary conditions on f, derived from conditions (A), (B) and (C) on ϕ, are

(i) $$\partial f / \partial \tau = 0 \quad \text{on} \quad \tau = 0, |\theta| \leqslant \gamma \tag{2.11}$$

(ii) $$f = 0 \quad \text{on} \quad \tau = 0, \gamma \leqslant |\theta| \leqslant \pi \tag{2.12}$$

(iii) $$f \text{ is an even function of } \theta. \tag{2.13}$$

Equation (2.10) has non-trivial solutions satisfying these boundary conditions for certain values of ν, and it is these eigenvalues which we proceed to calculate.

3. *Method of Solution.*

It is required to find the value of ν corresponding to a given value of γ such that a solution of equation (2.10) satisfying the boundary conditions (2.11) to (2.13) exists. The numerical method described here consists of using a transformation of variables to make the domain of the problem a rectangular region, in which the second order partial differential equation resulting from the transformation of variables is approximated by a finite difference representation on a rectangular mesh. This leads to a matrix equation which is satisfied when $\nu(\nu+1)$ is an eigenvalue of a specified matrix.

If an initial approximation to ν is known, the required eigenvalue of the matrix can be found accurately by an iterative process. The value of ν given by this method depends on the size of mesh used, and an accurate value of ν is found as the limit of a sequence of values of ν calculated for decreasing mesh sizes.

3.1. *The Problem in a Rectangular Domain.*

The transformation of the domain into a rectangular region is accomplished in two steps: first, the domain in the (τ, θ) plane is conformally mapped on to the interior of a circle, and then the latter is transformed non-conformally into a rectangular region.

The transformation of the domain into the interior of a circle with unit radius in a (w_1, w_2) co-ordinate system is accomplished by the series of conformal transformations defined by:

$$u = i(e^{\tau + i\theta} - \cos\gamma) \qquad \tau + i\theta = \log(-iu + \cos\gamma) \tag{3.1}$$

$$v = \left(\frac{\dfrac{u}{\sin\gamma} - i\tan\dfrac{\gamma}{2}}{1 - \dfrac{i\tan\dfrac{\gamma}{2}}{\sin\gamma}\,u} \right) = \frac{i\tanh\left(\dfrac{\tau+i\theta}{2}\right)}{\tan\dfrac{\gamma}{2}} \qquad u = \frac{\sin\gamma\left(v+i\tan\dfrac{\gamma}{2}\right)}{\left(1+iv\tan\dfrac{\gamma}{2}\right)} \tag{3.2}$$

$$w = v-(v^2-1)^{1/2} \qquad v = \frac{1}{2}\left(w+\frac{1}{w}\right) \tag{3.3}$$

where u, v and w are complex variables and $w = w_1 + iw_2$. The domain of the problem in the u, v and w co-ordinate systems are illustrated in Figs. 4, 5 and 6. It can be seen that the wing becomes the circumference of the circle in the (w_1, w_2) plane, and that, inside the circle, the areas $w_2 > 0, w_2 < 0, w_1 > 0, w_1 < 0$ correspond to the spaces in the physical plane $y_3 < 0$, $y_3 > 0$, $y_2 < 0$ and $y_2 > 0$. Thus, f is an even function of w_1 and an odd function of w_2, so we need consider only the first quadrant of the circle. We transform this into a rectangular region $0 \leqslant R \leqslant 1, 0 \leqslant \varphi \leqslant \pi/2$ by

$$w = Re^{i\varphi}, \tag{3.4}$$

the wing becoming the line $R = 1, 0 \leqslant \varphi \leqslant \pi/2$ (*see* Fig. 7), and the point A', corresponding to infinity upstream, becomes the line $R = 0, 0 \leqslant \varphi \leqslant \pi/2$.

The differential equation for f in R, φ co-ordinates is, from equation (2.10),

$$\cosh^2\tau \left|\frac{d(w_1+iw_2)}{d(\tau+i\theta)}\right|^2 \left\{\frac{\partial^2 f}{\partial R^2}+\frac{1}{R}\frac{\partial f}{\partial R}+\frac{1}{R^2}\frac{\partial^2 f}{\partial\varphi^2}\right\} + v(v+1)f = 0 \tag{3.5}$$

or

$$\psi(R,\varphi)\left\{\frac{\partial^2 f}{\partial R^2}+\frac{1}{R}\frac{\partial f}{\partial R}+\frac{1}{R^2}\frac{\partial^2 f}{\partial\varphi^2}\right\}+\lambda f = 0 \tag{3.6}$$

where

$$\lambda = v(v+1) \tag{3.7}$$

and

$$\psi(R,\varphi) = \cosh^2\tau \left|\frac{d(w_1+iw_2)}{d(\tau+i\theta)}\right|^2$$

which, after some manipulation, reduces to

$$\psi(R,\varphi) = \frac{\left(R^2+0{\cdot}25\,(R^4+2R^2\cos 2\varphi+1)\tan^2\dfrac{\gamma}{2}\right)^2}{(R^4+1-2R^2\cos 2\varphi)\tan^2\dfrac{\gamma}{2}}. \tag{3.8}$$

We obtain the boundary conditions on f from equations (2.11) to (2.13) and from considerations of symmetry:

(i) $\qquad f = 0 \quad$ on $\quad \varphi = 0, 0 \leqslant R \leqslant 1 \quad$ and on $\quad R = 0, 0 \leqslant \varphi \leqslant \pi/2$

(ii) $$\partial f/\partial R = 0 \quad \text{on} \quad R = 1, 0 \leqslant \varphi \leqslant \pi/2 \tag{3.9}$$

(iii) $$\partial f/\partial \varphi = 0 \quad \text{on} \quad \varphi = \pi/2, 0 \leqslant R \leqslant 1$$

3.2. *The Finite-Difference Representation.*

We obtain an approximate solution to equation (3.6) with boundary conditions (3.9) by considering a rectangular mesh over the domain and replacing the differential equation by a finite-difference equation at each grid point of the mesh. This gives a homogeneous system of linear equations in the values of f at the grid points, for which $\lambda = \nu(\nu+1)$ is an eigenvalue.

We consider a rectangular mesh with m intervals between $R = 0$ and $R = 1$, the $m+1$ grid lines being numbered from $p = 0$ (corresponding to $R = 0$) to $p = m$ (corresponding to $R = 1$), and l intervals between $\varphi = 0$ and $\varphi = \pi/2$, these grid lines being numbered from $q = 0$ to $q = l$. As f is zero when p or q is zero, we need consider equation (3.6) only at the $(m \times l)$ grid points given by $1 \leqslant p \leqslant m, 1 \leqslant q \leqslant l$. We denote the values of f and ψ at the intersection of the pth and qth grid lines by f_r and ψ_r where $r = p+(q-1)\,m$, as illustrated in Fig. 7.

For a mesh with evenly spaced grid lines we use the finite-difference approximations

$$\frac{\partial f}{\partial x}(x_1) = \frac{f(x_2)-f(x_0)}{2h} \tag{3.10}$$

$$\frac{\partial^2 f}{\partial x^2}(x_1) = \frac{f(x_2)+f(x_0)-2f(x_1)}{h^2} \tag{3.11}$$

where $h = x_2-x_1 = x_1-x_0$. Then at each interior point of the grid, equation (3.6) can be replaced by the equation

$$A_r f_{r-m}+B_r f_{r-1}+C_r f_r+D_r f_{r+1}+A_r f_{r+m} = \lambda f_r \tag{3.12}$$

for $$2 \leqslant p \leqslant m-1$$

$$2 \leqslant q \leqslant l-1$$

and where

$$A_r = -\frac{4l^2}{p^2\pi^2} m^2 \psi_r \tag{3.13}$$

$$B_r = -m^2 \psi_r \left(1-\frac{1}{2p}\right) \tag{3.14}$$

$$D_r = -m^2 \psi_r \left(1+\frac{1}{2p}\right) \tag{3.15}$$

$$C_r = m^2 \psi_r \left(2+\frac{8l^2}{p^2\pi^2}\right). \tag{3.16}$$

At points on the boundary of the grid, the approximating equation must take the boundary conditions (3.9) into account. The condition of zero normal derivative is satified by introducing a point outside the mesh with the same value as at the corresponding point inside, i.e. by putting

$$f_{r+m} = f_{r-m} \qquad \text{when } q = l$$

$$f_{r+1} = f_{r-1} \qquad \text{when } p = m \qquad \text{in equation (3.12)}$$

Thus we obtain the equations:

$$\begin{aligned}
&C_r f_r + D_r f_{r+1} + A_r f_{r+m} = \lambda f_r && \text{when } p = 1, q = 1\\
B_r f_{r-1} \quad &+ C_r f_r + D_r f_{r+1} + A_r f_{r+m} = \lambda f_r && \text{when } 2 \leqslant p \leqslant m-1, q = 1\\
(B_r + D_r) f_{r-1} &+ C_r f_r + A_r f_{r+m} = \lambda f_r && \text{when } p = m, q = 1\\
A_r f_{r-m} \quad &+ C_r f_r + D_r f_{r+1} + A_r f_{r+m} = \lambda f_r && \text{when } p = 1, 2 \leqslant q \leqslant l-1\\
A_r f_{r-m} + (B_r + D_r) f_{r-1} &+ C_r f_r + A_r f_{r+m} = \lambda f_r && \text{when } p = m, 2 \leqslant q \leqslant l-1\\
2A_r f_{r-m} \quad &+ C_r f_r + D_r f_{r+1} = \lambda f_r && \text{when } p = 1, q = l\\
2A_r f_{r-m} + B_r f_{r-1} \quad &+ C_r f_r + D_r f_{r+1} = \lambda f_r && \text{when } 2 \leqslant p \leqslant m-1, q = l\\
2A_r f_{r-m} + (B_r + D_r) f_{r-1} &+ C_r f_r = \lambda f_r && \text{when } p = m, q = l.
\end{aligned} \tag{3.17}$$

Similar equations to (3.12) and (3.17) are obtained if the lengths of the mesh intervals are unequal. Some calculations were made using intervals of equal length along the φ axis and of unequal length along the R axis, and the equations for the finite difference approximations and the coefficients A_r, B_r, C_r and D_r for this case are given in Appendix A.

The equations (3.12) and (3·17) lead to the matrix equation

$$(E_0 - \lambda I)\,\mathbf{f} = 0 \tag{3.18}$$

where $\{\mathbf{f}\}$ is the vector $(f_1, f_2, \ldots f_{ml})$,
I is the unit matrix, and E_0 is a square matrix of order ml with non-zero elements along five diagonals only. The form of E_0 is shown in Fig. 8.

A non-trivial solution for $\mathbf{f}$ requires that

$$\det |E_0 - \lambda I| = 0 \tag{3.19}$$

i.e. that λ is an eigenvalue of the matrix E_0.

3.3. *Details of Calculation.*

A computer programme has been written in ICL 1900 Fortran to calculate the elements of the matrix E_0 and find its required eigenvalue λ for input values of γ, m and l.

The calculation of the matrix E_0 is straightforward from the equations (3.13) to (3.16), (3.8) and Fig. 8. A good estimate λ_0 of λ can be made from the behaviour and series expansions of v already known. The values taken for λ_0 in the various cases calculated are given in the following table:

Case		Value of λ_0 calculated from
ν_0	$0 \leqslant \gamma < \pi/4$	series expansion[4] from $\gamma = 0$ for ν
	$\pi/4 \leqslant \gamma \leqslant \pi/2$	four term series expansion[4] from $\gamma = \pi/2$ for ν
	$\pi/2 \leqslant \gamma \leqslant \pi$	linear approximation $\nu = 1-\gamma/\pi$
ν_1	$0 \leqslant \gamma \leqslant \pi/2$	estimate based on ν_0
	$\pi/2 \leqslant \gamma \leqslant \pi$	approximation $\nu = 1+0{\cdot}5 \sin\gamma$

λ can then be calculated accurately in the following way.

If we consider the matrix

$$E = E_0 - \lambda_0 I\,, \tag{3.20}$$

then provided λ_0 is sufficiently close to λ, the eigenvalue of E, μ, with smallest modulus will be given by

$$\mu = \lambda - \lambda_0 \tag{3.21}$$

so

$$\lambda = \mu + \lambda_0\,. \tag{3.22}$$

The value of μ is obtained by Inverse Iteration[5]. This is a repetitive process, the ith stage being the calculation of the vector $\mathbf{y}^{(i)}$ from

$$E\,\mathbf{y}^{(i)} = \mathbf{y}^{(i-1)} \tag{3.23}$$

where $\mathbf{y}^{(0)}$ is arbitrary. For i sufficiently large

$$\mathbf{y}^{(i)} = \mu^{-i}(\bar{\mathbf{y}} + \mathbf{e}^{(i)}) \tag{3.24}$$

where $\bar{\mathbf{y}}$ is a constant vector and $\boldsymbol{\varepsilon}^{(i)}$ a vector with very small components. In practice, the vector $\mathbf{y}^{(i)}$ is normalised during each iteration to prevent accumulator overflow. This process has been found to give μ as accurately as required for i about four.

The calculation of the inverse of E for use in equation (3.23) is not feasible in view of the large size of E, which has $m^2 \times l^2$ elements. Instead, we decompose E into the product of a block upper triangular matrix U and a lower triangular matrix L with unit diagonal elements, i.e. put

$$E = LU\,. \tag{3.25}$$

Equation (3.23) can now be written

$$LU\,\mathbf{y}^{(i)} = \mathbf{y}^{(i-1)} \tag{3.26}$$

or, using a dummy vector $\mathbf{z}$,

$$L\,\mathbf{z} = \mathbf{y}^{(i-1)} \tag{3.27}$$

$$U\,\mathbf{y}^{(i)} = \mathbf{z}\,. \tag{3.28}$$

$\mathbf{z}$ and thence $\mathbf{y}^{(i)}$ can now be found by back substitution in equations (3.27) and (3.28).

Further savings in computer time and storage are gained by using the sparseness of the matrix E to write it, L and U as matrices of order l with submatrices of order m as elements. Then only $\{(2l-1)\,m^2+ml\}$ elements of E need be stored in the computer and matrix operations are carried out on matrices of order m^2 only. Further details of these calculations are given in Appendix B, and a flow diagram of the programme is given in Fig. 9.

The programme was generally used with a square mesh, i.e. with $l = m$. For a specific γ, the value of μ calculated by the programme will only approximate to the true value Υ say, owing to the finite difference approximation of equation (3.6), the difference between μ and Υ decreasing as l is increased. In practice, the magnitude of l is limited by computer storage restrictions, and a value for Υ is obtained by extrapolation from a sequence of values of μ calculated for increasing values of l.

The variation of μ with l was found to be approximately

$$\mu \sim cl^{-k}+\Upsilon \tag{3.29}$$

for l greater than some l_0, where c and k are constants for a particular γ and $k \geqslant 2$. Υ can thus be found using equation (3·29) to extrapolate to $l = \infty$. Then, by equation (3.22),

$$\lambda = \Upsilon+\lambda_0 \tag{3.30}$$

and hence ν can be found from

$$\nu = (0{\cdot}25+\lambda)^{1/2}-0{\cdot}5\,. \tag{3.31}$$

4. *Results.*

4.1. *The Singularity in the Loading at the Apex.*

For values of γ near $\pi/2$, the variation of μ with $l\,(=m)$ could be closely approximated by an equation of the form (3.29), and so an extrapolation to give Υ and hence ν_0 could be made with confidence. However, for small values of γ, the dependence of μ on l valid for large l could not be established from the results obtained with l limited by storage restrictions, and so no extrapolation was attempted. Some calculations were made at $\gamma = 27°$ with different numbers of mesh intervals l and m, and with mesh intervals of unequal length along the R axis, but these did not enable the extrapolation to be made more accurately. In Figs. 10a and 10b, the values of ν_0 for different mesh sizes $l\,(=m)$ are plotted, together with the extrapolated value of ν_0 as a dotted line, for each value of γ.

Values of ν_0 for different angles γ and the largest value of $l\,(=m)$ used are given in Table 2. The column on the right gives ν_0 calculated from the extrapolated value Υ, the variation of ν_0 with γ being shown graphically in Fig. 11. These results for $\gamma \leqslant \pi/2$ are also included in Table 1 for comparison with values obtained by different methods. The data of Table 1 is presented graphically in Fig. 12. It can be seen that the present method gives results in good agreement with the four-term series expansion near $\pi/2$, and with the values calculated numerically by Brown and Stewartson[4], but that the method cannot be used for small values of γ.

4.2. *The Loading at the Trailing Edge.*

The rate at which the loading tends to zero at the trailing-edge centre-section is determined by ν_1. Values of ν_1 have been calculated for a wide range of values of γ corresponding to swept-back trailing edges ($\gamma > \pi/2$), and for two values corresponding to forward sweep ($\gamma < \pi/2$), and these results are given in Table 3 together with the value of ν_1 calculated by the programme for the largest mesh size $l\,(=m)$ used. The variation of ν_1 with γ is shown graphically in Fig. 13.

Fig. 14 gives for each sweepback angle considered a graph of values of ν_1 calculated for different mesh sizes $l\,(=m)$ together with the extrapolated value ν_1 as a dotted line.

As in the calculation of ν_0 for small γ, values of ν_1 for γ near to π could not be found with certainty

as the extrapolation to give Υ could not be made reliably.

A search for other eigenvalues ν_m in the interval (1, 2) was made by calculating the eigenvalue closest to each of a range of numbers covering the interval (1, 2). This established that ν_1 was the only eigenvalue in this interval. It was also noted that, in general,

$$\nu_1(\gamma) \neq 1+\nu_0(\gamma),$$

although there is equality for $\gamma = 0$, $\pi/2$ and π.

5. *Conclusions.*

(a) According to linearised theory, the velocity potential has a singular behaviour near a kink in an edge of the planform of a lifting wing. For kinks at the leading and trailing edges of the centre-section, this behaviour is related to that of the flow past an infinite sector.

(b) The strength of the singularity in the loading at the apex of the wing has been calculated for a wide range of angles of sweepback. These results are in good agreement with series expansions[2,3,4] previously obtained and with the numerical results calculated by Brown and Stewartson[4].

(c) The way in which the loading tends to zero at the trailing edge of the centre-section has also been calculated for a wide range of angles of sweepback of the trailing edge and for two cases of forward sweep.

APPENDIX A

Equations for a Mesh with Intervals of Unequal Length.

Consider a mesh with intervals of equal length along the φ axis and of unequal length along the R axis. Let the length of the pth interval on the R axis be t_p/m. Then the distance to the pth grid line is $\frac{1}{m}\sum_{i=1}^{p} t_i$ and $\sum_{i=1}^{m} t_i = m$.

We use the finite difference approximations

$$\frac{\partial f}{\partial x}(x_1) = \frac{1}{(h_1+h_2)}\left(\frac{h_1}{h_2}f(x_2)-\frac{h_2}{h_1}f(x_0)\right)-\frac{(h_1-h_2)}{h_1 h_2}f(x_1)$$

$$\frac{\partial^2 f}{\partial x^2}(x_1) = \frac{2}{(h_1+h_2)}\left(\frac{f(x_0)}{h_1}+\frac{f(x_2)}{h_2}\right)-\frac{2f(x_1)}{h_1 h_2}$$

where $h_1 = x_1-x_0$, $h_2 = x_2-x_1$. These expressions reduce to those in (3.10) and (3.11) for $h_1 = h_2$. The boundary condition on $R = 1$ is satisfied by putting

$$t_{m+1} = t_m$$

and

$$f_{r+1} = f_{r-1} \qquad \text{for } p = m.$$

The equations (3.12) and (3.17) still apply in this case, but with modified expressions for the coefficients:

$$A_r = -\frac{4m^2\psi_r l^2}{\left[\sum_{i=1}^{p} t_i\right]^2 \pi^2}$$

$$B_r = -\frac{m^2\psi_r}{t_p(t_p+t_{p+1})}\left\{2-\frac{t_{p+1}}{\sum_{i=1}^{p} t_i}\right\}$$

$$C_r = \frac{m^2\psi_r}{t_p t_{p+1}}\left\{2+\frac{(t_p-t_{p+1})}{\sum_{i=1}^{p} t_i}\right\}+\frac{8m^2\psi_r l^2}{\left[\sum_{i=1}^{p} t_i\right]^2 \pi^2}$$

$$D_r = -\frac{m^2\psi_r}{t_{p+1}(t_p+t_{p+1})}\left\{2+\frac{t_p}{\sum_{i=1}^{p} t_i}\right\}$$

Note that $(B_r+D_r) = -\frac{2m^2\psi_r}{t_m^2}$ when $p = m$.

APPENDIX B

Details of Programme.

The matrix E can be written in the form

$$\begin{pmatrix} H_1 & J_1 & 0 & 0 & 0 & \cdots \\ J_2 & H_2 & J_2 & 0 & 0 & \cdots \\ 0 & J_3 & H_3 & J_3 & 0 & \cdots \\ \cdot & \cdot & \ddots & \ddots & \ddots & \\ \cdot & \cdot & \ddots & \ddots & J_{l-1} & \\ \cdot & \cdot & \cdot & J_l & H_l & \end{pmatrix} \tag{B.1}$$

where the H's and J's are submatrices of order m, the H's being tridiagonal, and the J's diagonal (*see* Fig. 8). Similarly the matrices L and U have the form

$$L = \begin{pmatrix} I & 0 & 0 & 0 & \cdots \\ L_1 & I & 0 & 0 & \cdots \\ 0 & L_2 & I & 0 & \cdots \\ 0 & 0 & L_3 & I & \cdots \\ \cdot & \cdot & \ddots & \ddots & \\ \cdot & \cdot & \ddots & I & \\ \cdot & \cdot & L_{l-1} & & \end{pmatrix} \quad U = \begin{pmatrix} U_1 & J_1 & 0 & 0 & \cdots \\ 0 & U_2 & J_2 & 0 & \cdots \\ 0 & 0 & U_3 & J_3 & \cdots \\ \cdot & \cdot & \ddots & \ddots & \\ \cdot & \cdot & \ddots & J_{l-1} & \\ \cdot & \cdot & U_{l-1} & & \\ \cdot & \cdot & & U_l & \end{pmatrix} \tag{B.2}$$

where the U's and L's are submatrices of order m but have no special form.

From equation (3.25) $E = LU$

hence

$$U_1 = H_1 \tag{B.3}$$

$$\left.\begin{aligned} L_{s-1} &= J_s U_{s-1}^{-1} \\ U_s &= H_s - L_{s-1} J_{s-1} \end{aligned}\right\} \text{ for } s = 2 \ldots l. \tag{B.4, B.5}$$

Thus only the U_s and L_s matrices and the diagonal elements of the J_s matrices need to be stored in the computer to record the matrix E.

It is then convenient to formulate the back-substitution calculations (3.27) and (3.28) in terms of the U_s, L_s and J_s matrices. Let $\{a\}$ be the transpose of a column vector a and denote

$$\begin{aligned} \{\mathbf{y}^{(i-1)}\} &= (\{v_1\}, \{v_2\}, \ldots, \{v_l\}) \\ \{\mathbf{z}\} &= (\{z_1\}, \{z_2\}, \ldots, \{z_l\}) \\ \{\mathbf{y}^{(i)}\} &= (\{y_1\}, \{y_2\}, \ldots, \{y_l\}) \end{aligned} \tag{B.6}$$

where v_s, z_s and y_s, $1 \leqslant s \leqslant l$, are $m \times 1$ column vectors. Then the back substitution

$$L\mathbf{z} = \mathbf{y}^{(i-1)} \tag{3.27}$$

is done using the formulae

$$\begin{aligned} z_1 &= v_1 \\ z_s &= v_s - L_{s-1} z_{s-1} \qquad \text{for} \quad s = 2, \ldots l, \end{aligned} \tag{B.7}$$

and the back substitution

$$U\mathbf{y}^{(i)} = \mathbf{z} \tag{3.28}$$

using the formulae

$$\begin{aligned} y_l &= U_l^{-1} z_l \\ y_s &= U_s^{-1} (z_s - J_s y_{s+1}) \qquad \text{for} \quad s = (l-1), \ldots 1 . \end{aligned} \tag{B.8}$$

We note that the inverses of the matrices U_s and not the matrices themselves are required in the calculations (B.4) and (B.8), and so immediately after the calculation of each U_s from (B.3) and (B.5) the inverse of the matrix is found and stored in place of the matrix.

The interation is begun using a unit column vector as $\mathbf{y}^{(0)}$, and thereafter each $\mathbf{y}^{(i-1)}$ is normalised with respect to its largest element. Thus, after the ith iteration the current estimate of μ is the inverse of the element of $\mathbf{y}^{(i)}$ of largest modulus. The iteration is continued until the difference between two successive estimates of μ is smaller than some value specified by the programmer. The rate of convergence to μ depends mainly on the ratio of μ to the eigenvalue of E with next smallest modulus, and, therefore, on the closeness of the approximation λ_0 to λ. In practice, convergence was rapid and occurred for i about 4.

LIST OF SYMBOLS

A_r, B_r, C_r, D_r		Coefficients in finite difference equation (3.12), defined in equations (3.13), (3.14), (3.16) and (3.15) respectively
E		Matrix, $= E_0 - \lambda_0 I$
E_0		Matrix, *see* equation (3.18) and Fig. 8
$f, f_m(\vartheta, \omega)$		Functions describing factor of ϕ, ϕ_m respectively
f_r		Value of f at rth grid point
$\mathbf{f}$		Column vector $\{f_1, \ldots, f_{ml}\}$
H_s		Submatrices of E for $s = 1, \ldots, l$
i		Iteration counter
I		Unit matrix
J_s		Diagonal submatrices of E for $s = 1, \ldots, l$
l		Number of intervals in mesh along φ axis
L		Lower triangular matrix
L_s		Submatrices of L for $s = 1, \ldots, l-1$
m		Number of intervals in mesh along R axis
p, q		Counters for numbering grid lines along R and φ axes, respectively
r	$=$	$(y_1^2 + y_2^2 + y_3^2)^{1/2}$
		also, $= p + (q-1)\,m$
R	$=$	$\lvert W \rvert$
t_p		m times length of pth interval on R axis
u		Complex co-ordinate defined in equation (3.1)
U		Block upper triangular matrix
U_s		Submatrices of U for $s = 1, \ldots, l$
v		Complex co-ordinate defined in equation (3.2)
v_s, y_s, z_s		$m \times 1$ column vector elements of $\mathbf{y}^{(i-1)}$, $\mathbf{y}^{(i)}$ and $\mathbf{z}$
$w = w_1 + iw_2$		Complex co-ordinates defined in equation (3.3)
x_1, x_2, x_3		Physical Cartesian co-ordinates, *see* Fig. 1
y_1, y_2, y_3		Stretched co-ordinate system of sector problem, *see* equation (2.1) and Fig. 2
$\mathbf{y}^{(i)}$		Vector result of ith iteration
$\mathbf{z}$		Dummy vector
α		Slope of camber surface of wing
γ		Semi-apex angle of sector
Υ		True value of μ
ε		Parameter of co-ordinate stretching, *see* equation (2.1)

LIST OF SYMBOLS—*continued*

θ, τ		Co-ordinate system of Legendre, *see* equation (2.7)
λ	=	$\nu(1+\nu)$
λ_m	=	$\nu_m(1+\nu_m)$
λ_0		Approximate value of λ
μ	=	$\lambda-\lambda_0$
ν, ν_m		Exponents of distance factor in eigensolutions ϕ, ϕ_m
ν_0		Smallest positive ν_m
ν_1		Second smallest positive ν_m
ϕ, ϕ_m		Velocity potential of sector problem
ϕ_ε		*See* equation (2.2)
Φ		Disturbance velocity potential of flow past wing
φ	=	$\arg(W)$
$\psi(R, \varphi)$		Function defined in equation (3.8)
ψ_r		Value of ψ at rth grid point

REFERENCES

No.	*Author(s)*	*Title, etc.*
1	P. Germain	Sur l'écoulement subsonique au voisinage de la pointe avant d'une aile delta. *La Recherche Aéronautique* No. 44, 3–8 (1955).
2	R. Legendre	Écoulement subsonique transversal à un secteur angulaire plan. *C.R. Acad. Sci.*, 26 November 1956, 1716–18.
3	J. P. Guiraud	Sur la nature de la singularité d'un écoulement de fluide compressible au voisinage de la pointe avant d'une aile delta en régime subsonique. *C.R. Acad. Sci.*, 17 December 1956, 2012–2014.
4	S. N. Brown and K. Stewartson	Flow near the apex of a plane delta wing. *Jl. I.M.A. 5*, 206–216, (1969).
5	L. Fox	*An introduction to numerical linear algebra.* Oxford, Clarendon Press, pp. 224–225 (1964).
6	R. Courant and D. Hilbert ..	*Methods of Mathematical Physics*, Vol. 1. New York, Interscience Publishers Inc. (1953).

TABLE 1

Values of v_0 Obtained by Different Methods.

γ° \ ν°	Four term series[4] expansion from $\gamma = \pi/2$	Series expansion[4] from $\gamma = 0$	Brown and Stewartson[4] numerical method	Present method
0	1·0049	1·0000		
9	0·9954	0·9936	0·9925*	
18	0·9678	0·9729	0·9733*	
27	0·9244	0·9344	0·9356*	0·933
36	0·8690	0·8747	0·8808*	0·880
45	0·8059	0·7946	0·8146	0·8145
54	0·7394	0·7189	0·7441*	0·7441
63	0·67334	0·7983	0·6749*	0·6749
72	0·6106	2·0386	0·6108*	0·6109
81	0·5526	17·245	0·5528*	0·5526
90	0·5000	∞		0·5000

*Interpolated using Lagrangian interpolation from values calculated at intervals of 15°.

TABLE 2

Values of v_0 Calculated by the Programme.

γ°	At largest mesh size $l (= m)$	v_0	Extrapolated values of v_0
9			
18	18	0·93147	
27	19	0·92474	0·933
36	18	0·87654	0·880
45	18	0·81256	0·8145
54	17	0·74262	0·7441
63	17	0·67416	0·6749
72	17	0·61037	0·6109
81	17	0·55229	0·5526
90	17	0·49980	0·5000
99	17	0·45227	0·4524
108	17	0·40894	0·4090
117	17	0·36907	0·3690
126	17	0·33191	0·3318
135	18	0·29672	0·2966
144	17	0·26276	0·2626
153	18	0·22898	0·229
162	17	0·19370	0·194
171	18	0·14724	0·15

TABLE 3

Values of v_1 Calculated by the Programme.

γ°	At largest $l(=m)$	mesh size v_1	Extrapolated value of v_1
45	18	1·58131	1·60
81	17	1·49569	1·501
99	17	1·49524	1·499
108	17	1·49058	1·495
117	17	1·47777	1·483
126	18	1·45427	1·461
135	18	1·41734	1·426
144	18	1·36786	1·382
153	19	1·30760	1·33
162	19	1·21277	1·26
171	18	0·89529	

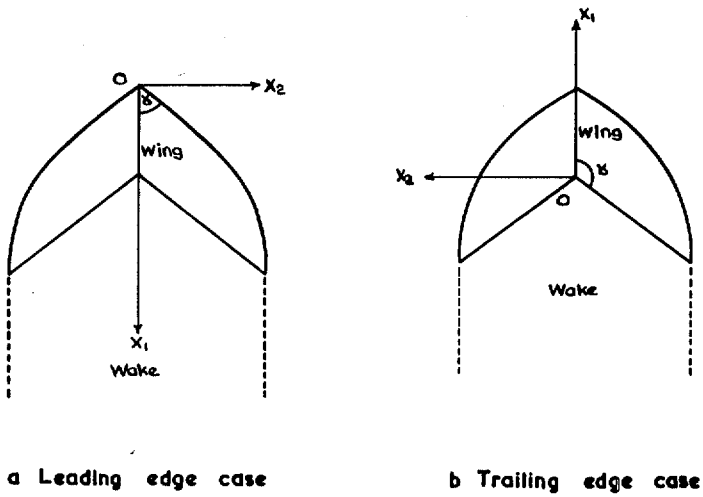

a Leading edge case

b Trailing edge case

FIG. 1 a & b. Planform and physical co-ordinate system.

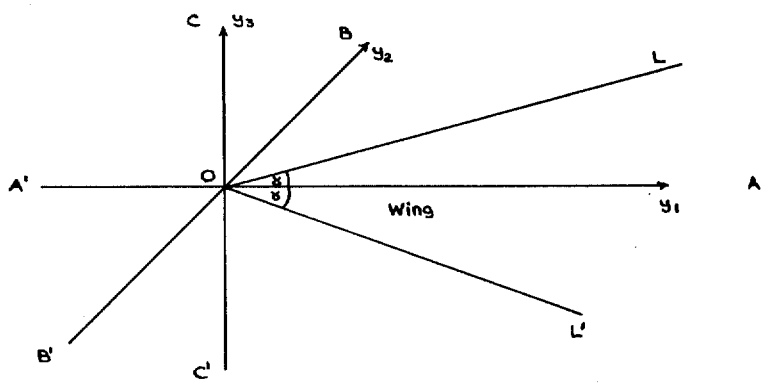

FIG. 2. Co-ordinate system for sector problem.

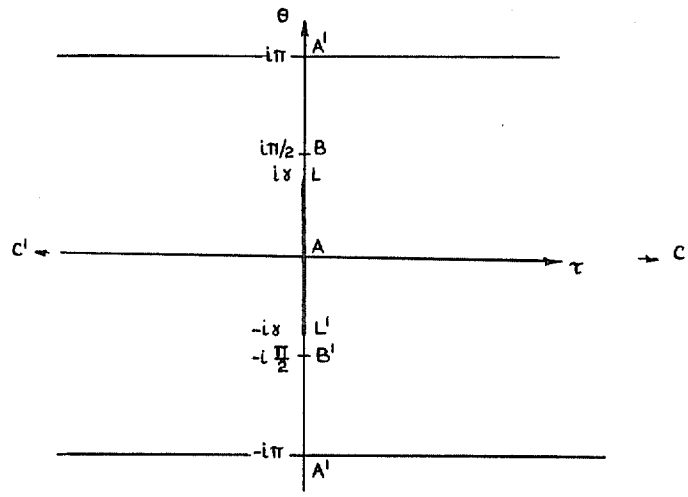

FIG. 3. (τ, θ) co-ordinate system of Legendre.

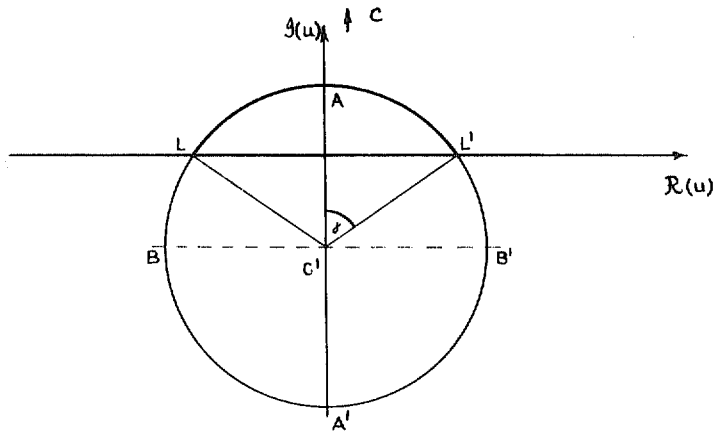

FIG. 4. u co-ordinate system.

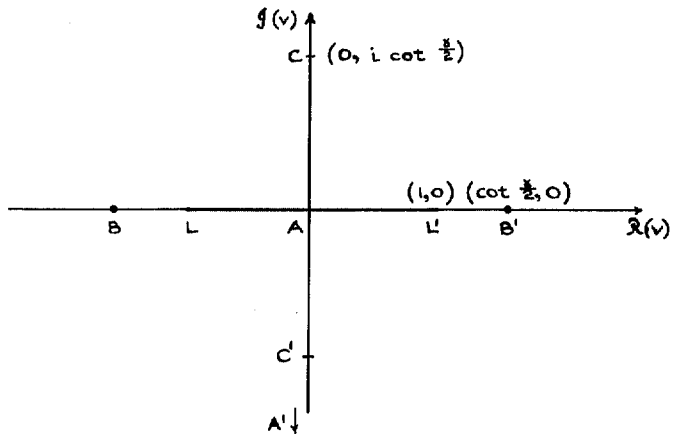

FIG. 5. v co-ordinate system.

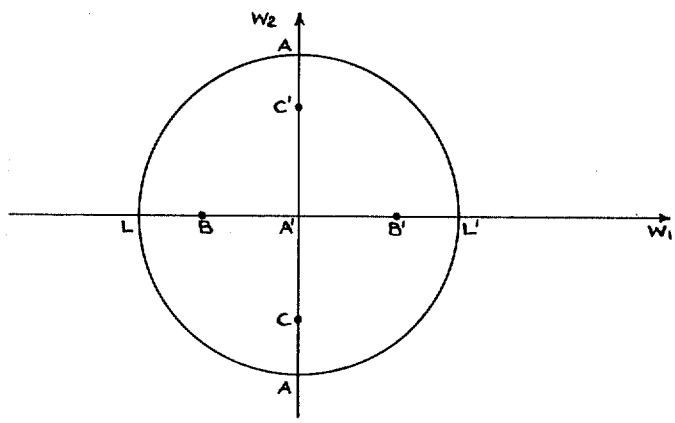

FIG. 6a. (w_1, w_2) co-ordinate system for $\gamma < \pi/2$.

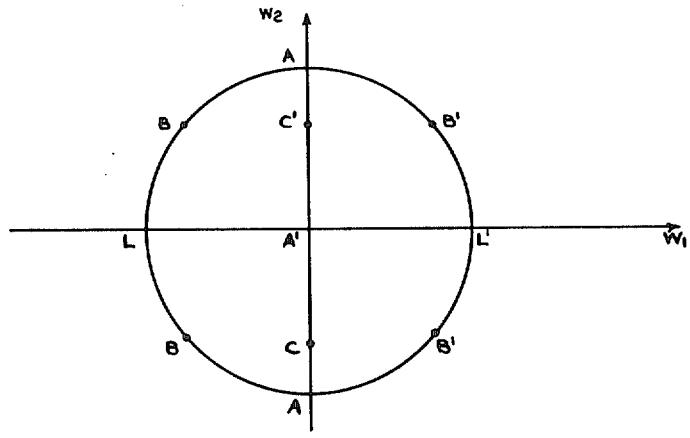

FIG. 6b. (w_1, w_2) co-ordinate system for $\gamma > \pi/2$.

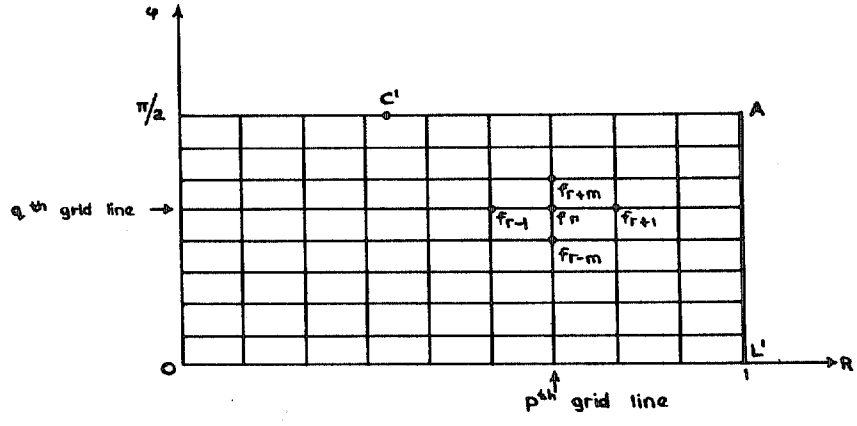

FIG. 7. The mesh in the R, φ plane.

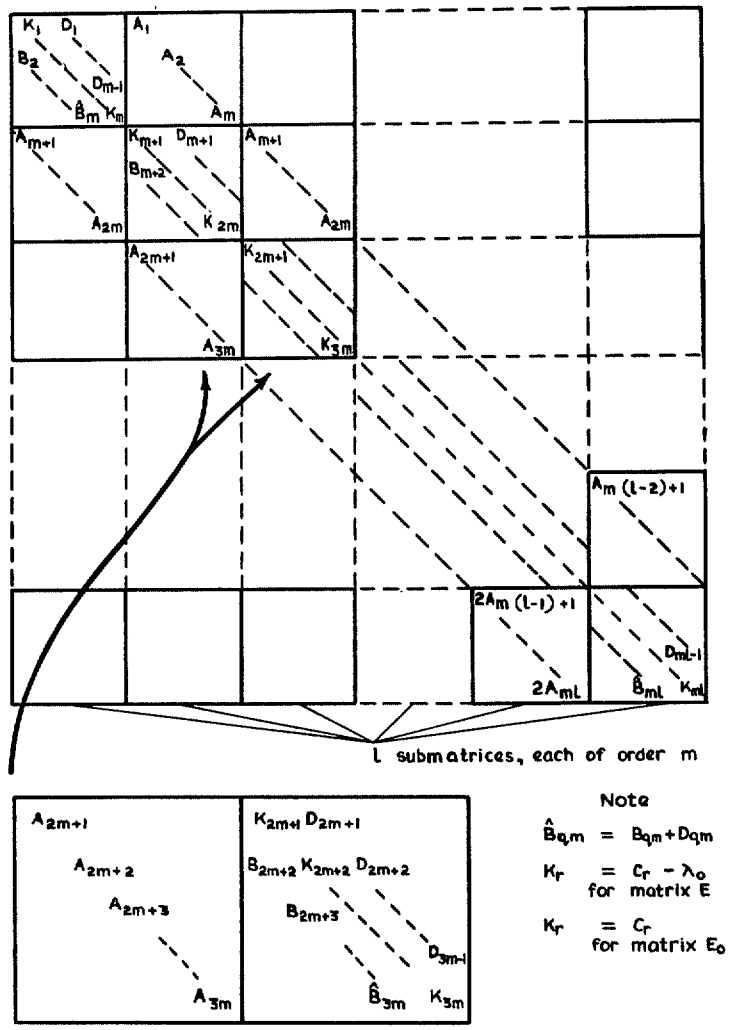

FIG. 8. The form of matrices E and E_0.

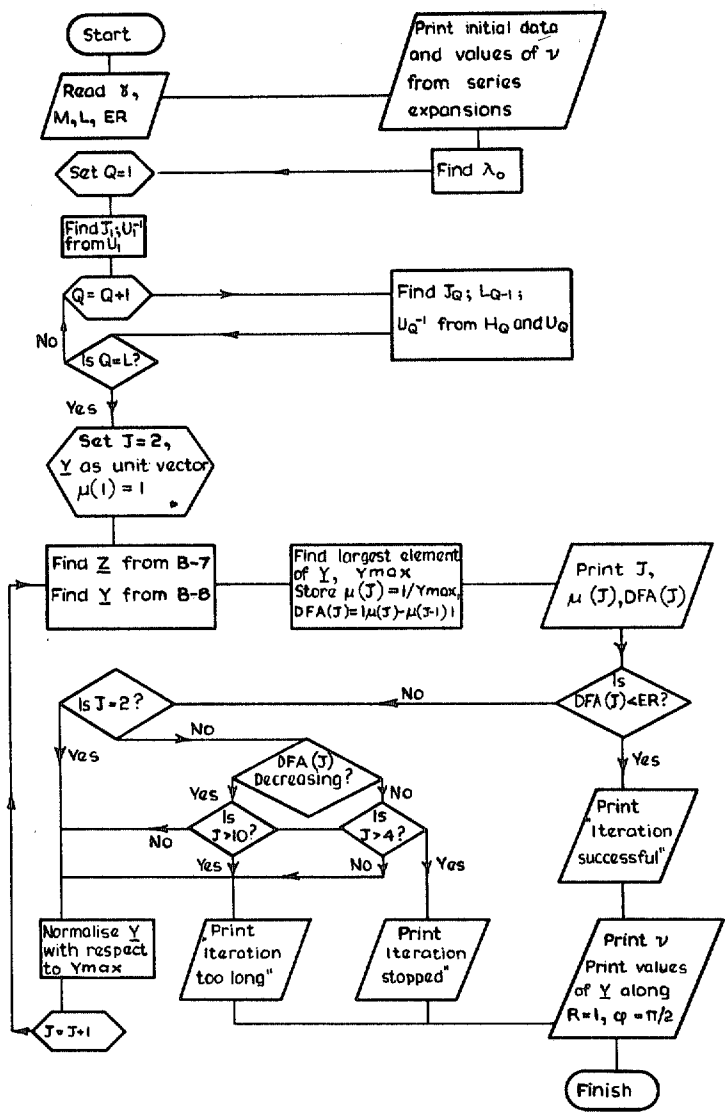

FIG. 9. Flow diagram of programme.

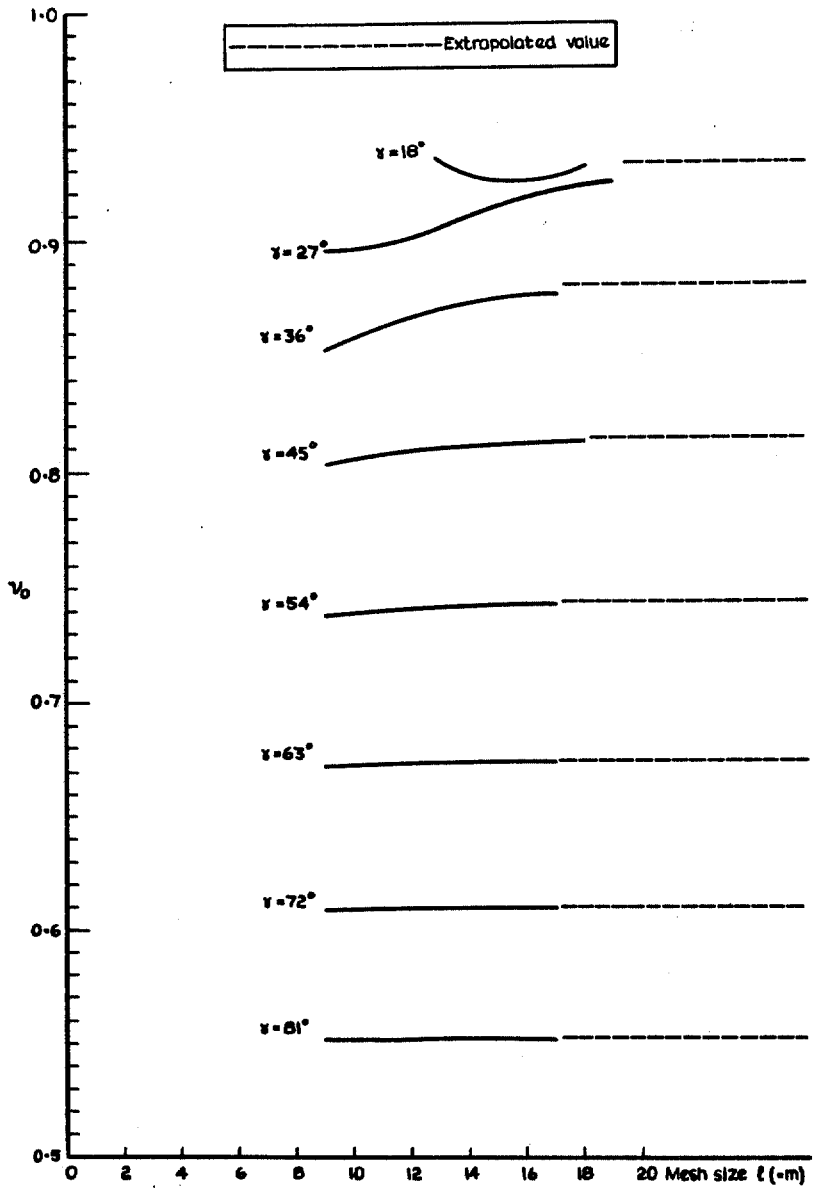

FIG. 10a. Graphs of ν_0 calculated for different mesh sizes.

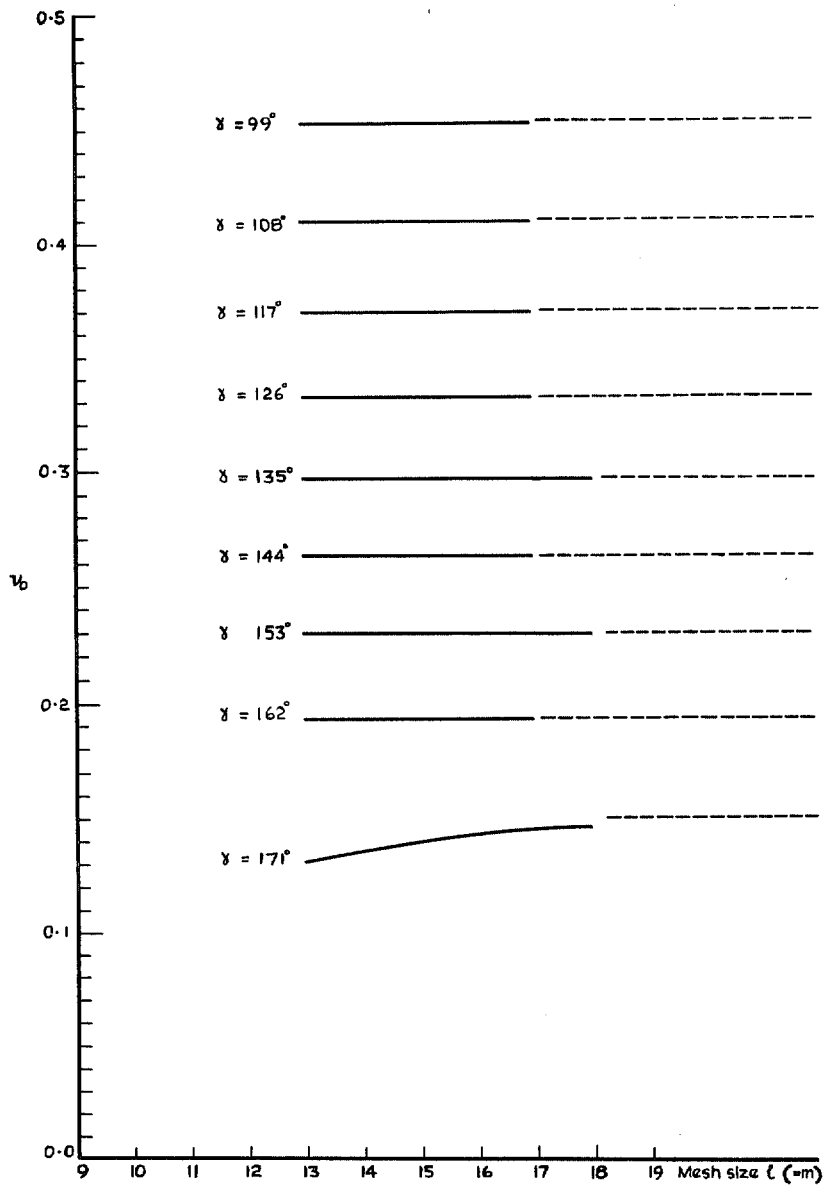

FIG. 10b. Graphs of ν_0 calculated for different mesh sizes.

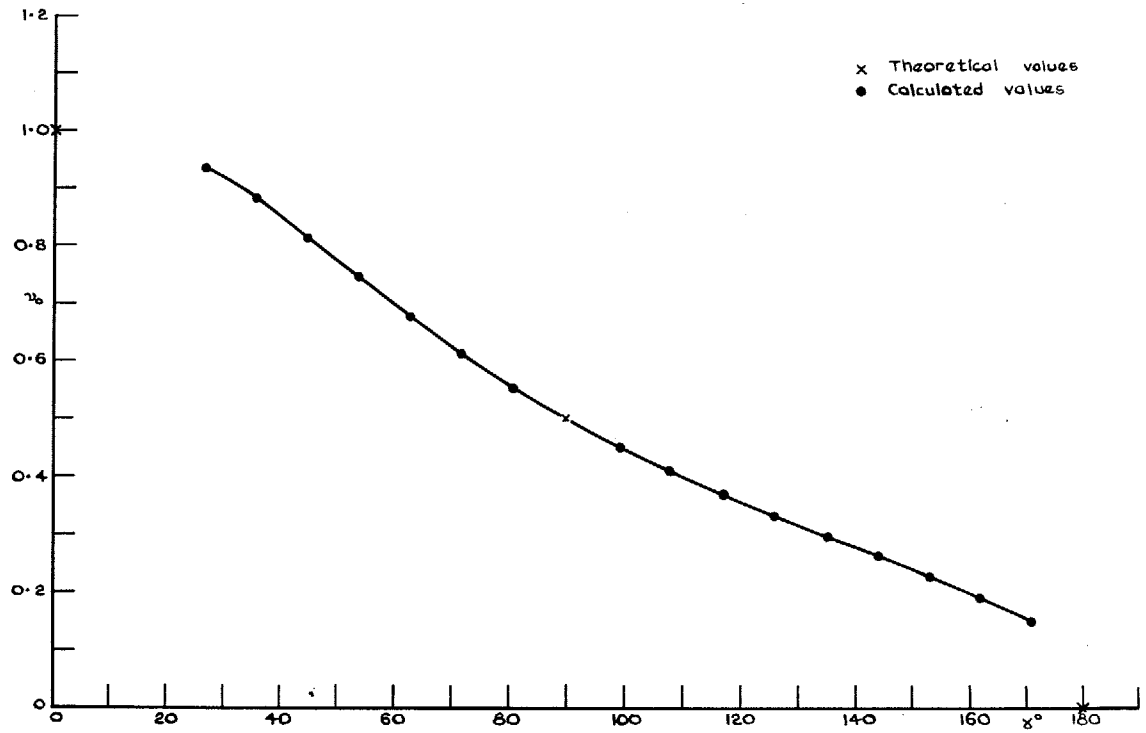

FIG. 11. Variation of v_0 with γ.

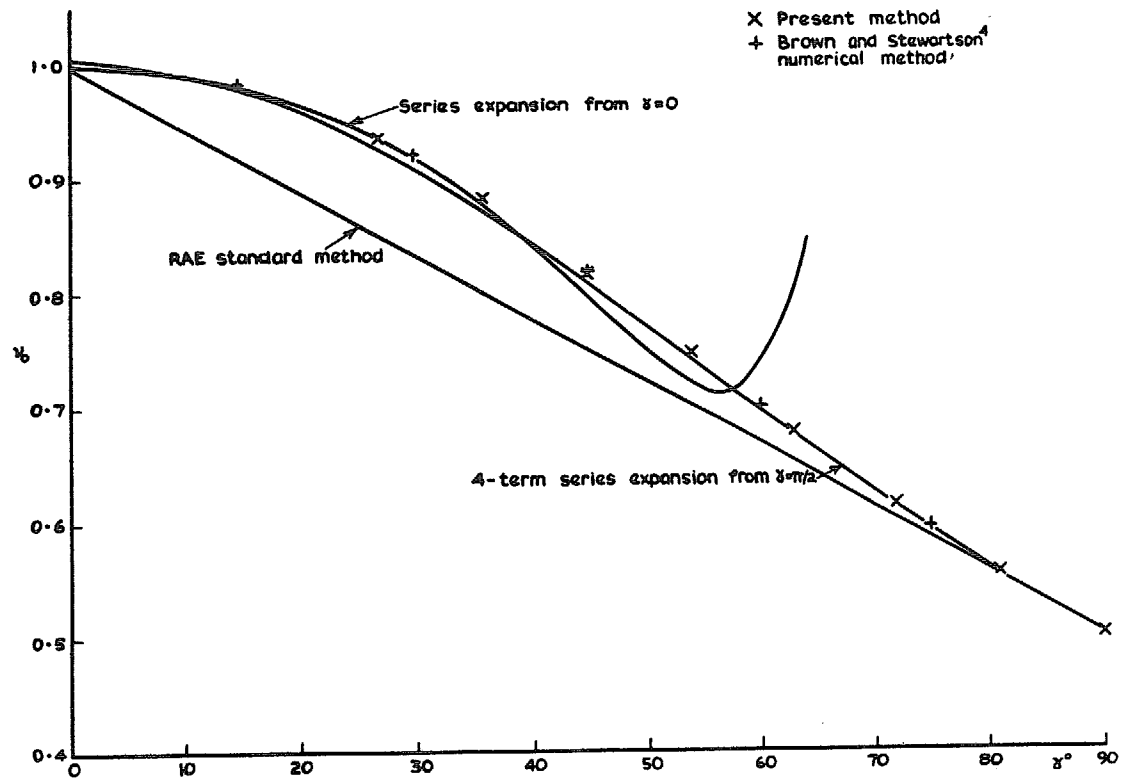

FIG. 12. Comparison of values of v_0 obtained by different methods.

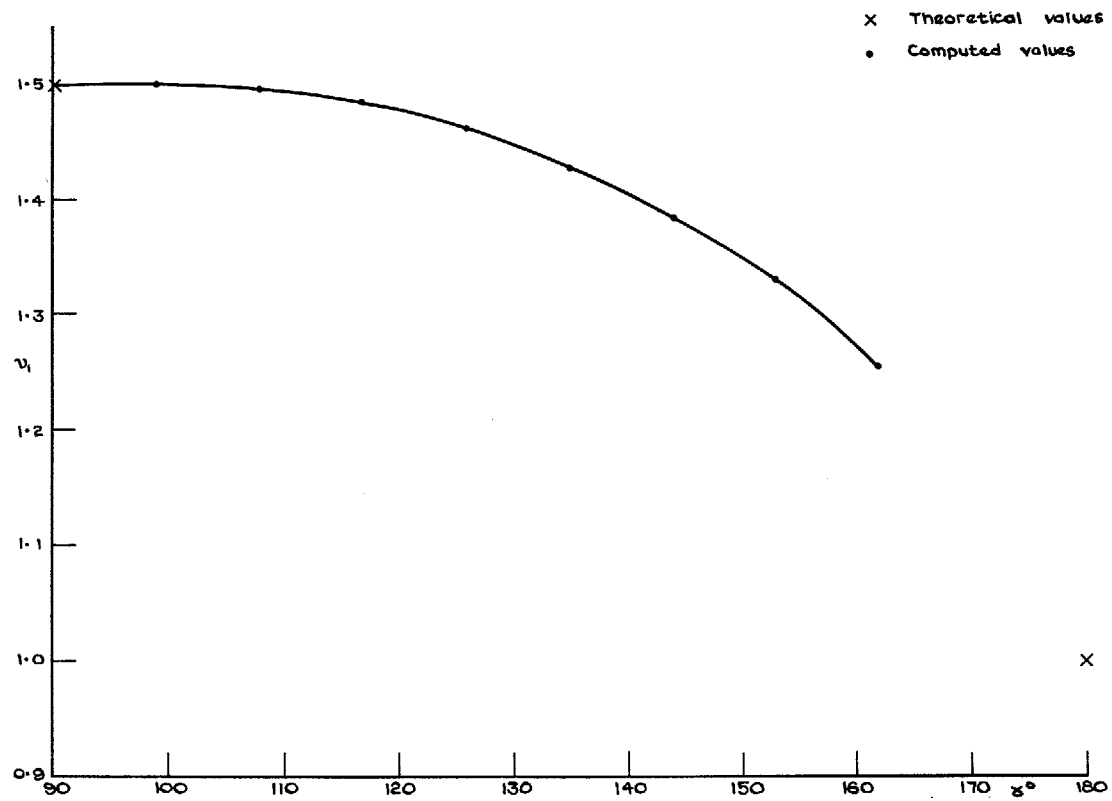

FIG. 13. Variation of v_1 with γ.

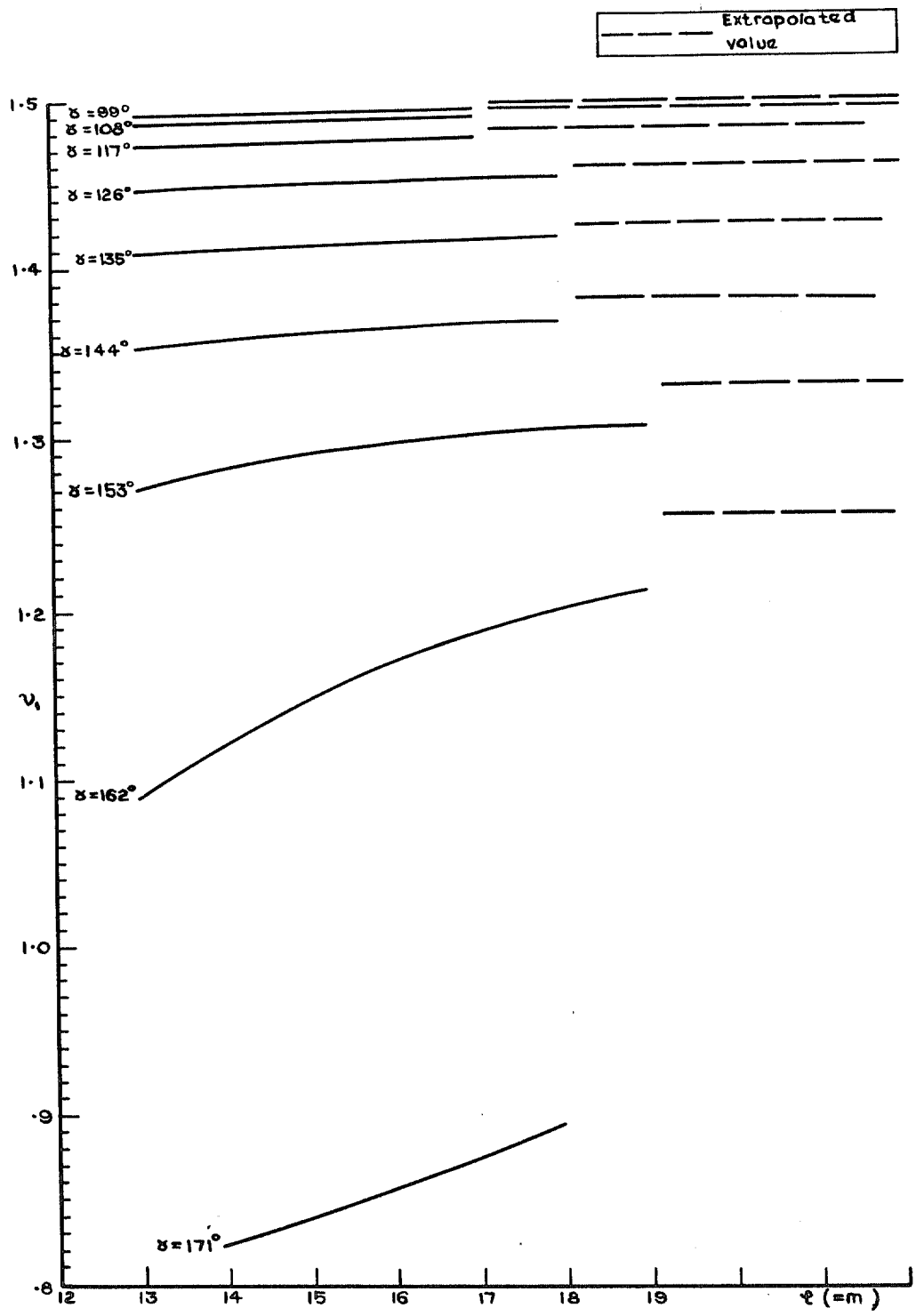

FIG. 14. Graphs of ν_1, calculated for different mesh sizes.

Printed in Wales for Her Majesty's Stationery Office by Allens Printers (Wales) Limited

Dd. 146916 K.5

© *Crown copyright* 1970

Published by
HER MAJESTY'S STATIONERY OFFICE

To be purchased from
49 High Holborn, London WC1
13a Castle Street, Edinburgh EH2 3AR
109 St Mary Street, Cardiff CF1 1JW
Brazennose Street, Manchester M60 8AS
50 Fairfax Street, Bristol BS1 3DE
258 Broad Street, Birmingham 1
7 Linenhall Street, Belfast BT2 8AY
or through any bookseller

R. & M. No. 3630
SBN 11 470330 2